

RSC Advances



This is an *Accepted Manuscript*, which has been through the Royal Society of Chemistry peer review process and has been accepted for publication.

Accepted Manuscripts are published online shortly after acceptance, before technical editing, formatting and proof reading. Using this free service, authors can make their results available to the community, in citable form, before we publish the edited article. This *Accepted Manuscript* will be replaced by the edited, formatted and paginated article as soon as this is available.

You can find more information about *Accepted Manuscripts* in the [Information for Authors](#).

Please note that technical editing may introduce minor changes to the text and/or graphics, which may alter content. The journal's standard [Terms & Conditions](#) and the [Ethical guidelines](#) still apply. In no event shall the Royal Society of Chemistry be held responsible for any errors or omissions in this *Accepted Manuscript* or any consequences arising from the use of any information it contains.

**One-dimension Graphene Nanoribbons Hybridized with Carbon Nanotubes as
Cathode and Anode Interfacial Layers for High Performance Solar Cells**

Yong Zhang^a, Yawen Liu^a, Lie Chen^{a,b}, Xiaotian Hu^a, Lin Zhang^a, Lin Hu^a, Yiwang
Chen^{*a,b}

^aCollege of Chemistry/Institute of Polymers, Nanchang University, 999 Xuefu
Avenue, Nanchang 330031, China

^bJiangxi Provincial Key Laboratory of New Energy Chemistry, Nanchang University,
999 Xuefu Avenue, Nanchang 330031, China

*Corresponding author. Tel.: +86 791 83968703; fax: +86 791 83969561. E-mail:
ywchen@ncu.edu.cn (Y. Chen).

Abstract

Solution processible graphene oxide nanoribbon (GONR) with continuously one-dimensional length and remaining carbon nanotubes (CNTs) have been synthesized by partially unzipping from multiwalled carbon nanotubes (MWCNTs). Such low-cost GONR hybridized with CNTs (GONR/CNTs) show solution processibility as well as tunable work function and multifunctional interfacial modification in the polymer solar cells (PSCs) due to well-defined nanoribbons containing CNTs with continuously one-dimensional length and promoting the charge transporting, different from the GONR unzipped from single-walled carbon nanotubes tending to form large amount of graphene oxide pieces. Incorporation of the GONR/CNTs into the solution processed PSCs as electron transporting layer (ETL) and hole transporting layer (HTL) simultaneously delivers a high device performance with long-term stability. The results demonstrate that the multifunctional GONR/CNTs unzipped from MWCNTs would be a promising interfacial materials for solution processed high performance PSCs.

Keywords: Graphene oxide nanoribbons; Carbon nanotubes; Work function; Polymer solar cells; Stability

1. Introduction

Owing to the advantage of roll-to-roll process, flexibility, lightweight and low cost, polymer solar cells (PSCs) is now drawing a great deal of interests as potential sources of renewable and clean energy.¹⁻⁵ It has been reported that PSCs based on bulk-heterojunction (BHJ) blends of organic donor and fullerene acceptor have achieved a considerably high power conversion efficiency of $\sim 11\%$,⁶ providing impetus for their successful commercialization.⁷⁻⁹

The interfacial layer between the electrode and active layer is crucial and even decisive for PSCs because of its function of electron/hole transporting and protection of devices out of efficiency degradation. Poly (3,4-ethylene dioxythiophene):(polystyrene sulfonic acid) (PEDOT:PSS), a commercial product, is widely used in PSCs and organic light emitting diode (OLED) devices. In general, the initially implemented BHJ conventional structure of PSCs is active layer sandwiched between the PEDOT:PSS coated indium tin oxide (ITO) and a low work function metal cathode (e.g. Al). But this conventional structure always suffers from cell degradation problems mainly by the reason of the acidic and hygroscopic nature of PEDOT:PSS corroding ITO substrate.

To avert the problem, the inverted structure is introduced, where air-stable high work function metal (such as Ag or Au) is used as the anode to collect holes while electron transporting layer (ETL) (such as zinc oxide (ZnO)) modified ITO acts as cathode to collect electrons. Stability is found to be improved with the inverted structure because ITO/PEDOT:PSS interface can be avoided and the air-stable high work function metal electrode serves to self-encapsulate the cells. Current state-of-the-art materials for ETLs include inorganic metal oxides, such as ZnO¹⁰ or titanium oxide (TiO_x).¹¹⁻¹⁴ However, in order to improve the crystallinity of the metal oxides to yield a high charge carrier mobility, conversion of precursor to metal oxide undergoes a high temperature (over 200 °C) annealing process, which limits its printable applications. To avoid the inherent weakness of inorganic material as ETLs, organic interlayer

materials, such as fullerene derivatives, self-assembled monolayers and conjugated polyelectrolytes (CPEs)¹⁵⁻¹⁷ have been employed, but most of them are required tedious synthesis.

The unique 2-dimensional carbon nanostructure with extraordinary electrical and optical properties and mechanical flexibility, graphene has attracted great interest in the scientific community. Its tunable work function properties also give rise to its utilization as various components in novel optoelectronic devices.¹⁸⁻²³ However, the poor processing limits graphene for widely application in PSCs due to the strong π -stacking interactions between graphene sheets and the lack of solubilizing functionalities and substituents on the structure. Massive researches on the production of solution processible graphene by exfoliation of graphite into graphene oxide (GO), has allowed the functionalization and processing of graphene flakes with various methods, triggering the large-scale production of graphene-based devices.²⁴⁻²⁸ But there is still a challenge for GO-based controllable electronic properties for high performance devices. The quasi-one-dimensional graphene oxide nanoribbon (GONR)²⁹ with a synergistic effect to have an opened bandgap like graphene nanoribbon (GNR) and the solution processibility of GO, has been attracted many interesting. The pristine graphene is a zero-bandgap material with metal-like conductivity, while GNR is a new class of semiconducting with an opened bandgap induced by the quasi-one-dimensional confinement of charge carriers.²⁹⁻³⁴ Dai's group first introduced the GONR unzipped from single-walled carbon nanotubes into the BHJ-based PSCs as hole transporting layer (HTL), and reached a relatively high performance.³⁵ Therefore, the GONR could be of the great potential for optoelectronic application.

Here, GONR hybridized with carbon nanotubes (CNTs) (GONR/CNTs) unzipped from multiwalled carbon nanotubes (MWCNTs) is first introduced into the invert PSCs as HTL and ETL simultaneously. MWCNTs used here are not only low cost but also can ensure well-defined nanoribbons contain carbon nanotubes with continuously

one-dimensional length after partially unzipping, allowing for a relatively high conductivity compared with pure GONR. Pristine GONR/CNTs as HTL and polyethylenimine, 80% ethoxylated (PEIE) modified GONR/CNTs as ETL³⁶ has been successfully applied in the invert devices based on poly(3-hexylthiophene):[6,6]-phenyl C61-butyric acid methyl ester (P3HT:PCBM) and poly{4,8-bis[(2-ethylhexyl)oxy]benzo[1,2-b:4,5-b']dithiophene-2,6-diyl-alt-3-fluoro-2-[(2-ethylhexyl)carbonyl]thieno[3,4-b]thiophene-4,6-diyl};[6,6]-phenyl C71-butyric acid methyl ester (PTB7:PC₇₁BM).

2. Experimental Section

2.1. Materials

ITO glass (<10Ω), P3HT (Rieke Metals Inc., Cat. No.: 4002-E, M_w=50000 g/mol, polydispersity: 2.0-2.4), PTB7 (1-Material Chemscitech Inc., Cat. No.: OS0007, M_w=138000 g/mol, polydispersity: 2.5), PC₆₁BM, PC₇₁BM (American Dye Source, Inc., 99.5%) were used as received. MWCNTs (diameter 40-60 nm) were purchased from XFNano Materials Tech Co., Ltd. (Nanjing, China).

2.2. Synthesis and Purification of GONR/CNTs

The GONR/CNTs were prepared according to the modified Tour method.³⁰ Typically, 150 mg of CNTs were suspended in 30 mL of concentrated sulfuric acid (H₂SO₄) (98%) by stirring for 3 h. Phosphoric acid (H₃PO₄) was then added, and the mixture was stirring another 15 min. After it, 500 mg of potassium permanganate (KMnO₄) was then added in five portions and stirred at room temperature for 2h. After the resulting mixture was heated at 65 °C for 2 h, extra KMnO₄ (250 mg) was added in several portions. Upon the reaction was finished, the mixture was naturally cooled to room temperature and subsequently poured in to 1 L of ice-water containing 15 mL H₂O₂ (30 wt%). Afterwards, the obtained samples were dialyzed in HCl and deionized water for one week. The resultant dispersion was centrifuged (20000 rpm, 20 min) to give crude GONR/CNTs as dark precipitate. Finally, the resultant dark precipitate was

dry in vacuum refrigerant dryer for 24 hours.

2.3. Device Fabrication

2.3.1. Conductivity measurement device fabrication. To research the conductivity of the GONR and GONR/CNTs, the device with the structure of ITO/GONR/Au and ITO/GONR/CNTs/Au were fabricated. GONR and GONR/CNTs solution were dropped on the ITO-coated substrate with slow drying in the air to achieve film with the thickness about 50 nm. And Au (100 nm) was thermal evaporating under 4×10^{-4} pa. The current-voltage scans were taken within the scope of -2 V to 2 V.

2.3.2. Polymer solar cell fabrication. ITO-coated glass substrates were first cleaned by ultrasonic agitation in acetone, detergent, deionized water, and isopropanol sequentially, followed by UV ozone treatment for 15 min. For the ETL fabrication, GONR/CNTs were spin-coated from its 3 mg mL^{-1} aqueous solution at 3000 rpm for 60 s to form 3 nm thickness film. After drying at hot plate $150 \text{ }^{\circ}\text{C}$ for 15 min, the PEIE was spin-coated on the top of GONR/CNTs at 5000 rpm for 60s followed by annealing at hot plate $100 \text{ }^{\circ}\text{C}$ for 10 min. For the reference ETL, ZnO precursor was prepared according to the Sol-Gel-Derived method.³⁷ Typically, zinc acetate dihydrate ($\text{Zn}(\text{CH}_3\text{COO})_2 \cdot 2\text{H}_2\text{O}$, Aldrich, 99.9%, 1 g) and ethanolamine ($\text{NH}_2\text{CH}_2\text{CH}_2\text{OH}$, Aldrich, 99.5%, 0.28 g) were dissolved in 2-methoxyethanol ($\text{CH}_3\text{OCH}_2\text{CH}_2\text{OH}$, Aldrich, 99.8%, 10 mL) under vigorous stirring for 12 h for the hydrolysis reaction in air. ZnO precursor solution was spin-coated at 4000 rpm for 60 s and then annealing at $200 \text{ }^{\circ}\text{C}$ for 1 h. The 1,2-dichlorobenzene solution of P3HT and PC_{61}BM (1:0.8 w/w, polymer concentration of 18 mg mL^{-1}) was then spin-coated on top of ETL films at 800 rpm for 30 s and 1400 rpm 2 s. After drying for 2 h, the film was annealed at $150 \text{ }^{\circ}\text{C}$ for 10 min in N_2 filled glove box. For PTB7: PC_{71}BM -based device, PTB7: PC_{71}BM with a nominal thickness of 180 nm, was prepared by spin-coating a mixed solvent of chlorobenzene/1,8-diiodooctane (97:3% by volume) solution (concentration, 25 mg mL^{-1}) at 1000 rpm for 2 min. For the HTL fabrication. The GONR/CNTs were spin-coated from its 2 mg mL^{-1} isopropanol solution at 2000 rpm 45 s to form 3 nm thickness film. For the reference HTL, MoO_3 (70 nm) was

evaporating under 4×10^{-4} pa. Finally, Ag (100 nm) was thermal evaporating under 4×10^{-4} pa through a shadow mask to form an active area of $\approx 4 \text{ mm}^2$.

2.4. Measurement

Current-voltage (J - V) characteristics were characterized using Keithley 2400. The currents were measured in the dark and under $100 \text{ mW} \cdot \text{cm}^{-2}$ simulated AM 1.5 G irradiation (Abet Solar Simulator Sun2000). All the measurements were performed under ambient atmosphere at room temperature. The incident photo-to-electron conversion efficiency spectrum (IPCE) were detected under monochromatic illumination (Oriel Cornerstone 260 1/4 m monochromator equipped with Oriel 70613NS QTH lamp), and the calibration of the incident light was performed with a monocrystalline silicon diode. The morphologies of P3HT:PC₆₁BM films were investigated by atomic force microscopy (AFM) using a Digital Instrumental Nanoscope 31 operated in the tapping mode. Transmission electron microscopy (TEM) imaging was performed on a JEOL JEM-2100F. Scanning electron microscopy (SEM) imaging was performed on FEI Quanta 200F. X-ray diffraction (XRD) measurements were performed with a Rigaku D/Max-B X-ray diffractometer with Bragg-Brentano parafocusing geometry, a diffracted beam monochromator, and a conventional cobalt target X-ray tube set to 40 KV and 30 mA. The ultraviolet-visible (UV) spectra of the samples were recorded on a PerkinElmer Lambda 750 spectrophotometer. X-ray photoelectron spectroscopy (XPS) studies were performed on a Thermo-VG Scientific ESCALAB 250 photoelectron spectrometer using a monochromated Al ($K\alpha$) (1,486.6 eV) X-ray source.

3. Results and Discussion

3.1 characteristics of GONR/CNTs

As shown in Figure 1a, GONR/CNTs were synthesized from oxidative unzipping of MWCNTs with KMnO_4 as oxidant in concentrated H_2SO_4 and H_3PO_4 , similar with the published procedure.^{29, 30} The process transformed the insoluble pristine MWCNTs to hydroxyls and carboxyls³⁸ functionalized GONR/CNTs that easily

dispersed in water or other polar organic solvent (such as dimethylformamide). Figure 1b shows a typical TEM image of tangled pristine MWCNTs with a diameter of 50 nm. After unzipping by KMnO_4 , the opened GONR (Figure 1c) looks like ribbon with a much broader width than pristine MWCNTs (with the average width of 95 nm), indicating a successful unzipping of MWCNTs. It should be noted that quite different from the GONR unzipped from single-walled carbon nanotubes tending to form large amount of GO pieces³⁵, the ones prepared from MWCNTs are only longitudinally unzipped along the axial of MWCNTs to develop well-defined nanoribbons containing carbon nanotubes with continuously one-dimensional length and promoting the charge transporting.²⁹ The nanoribbon is also verified by the SEM image of GONR (Figure S1). Moreover, comparison of the insets in Figure 1b and 1c, the pristine MWCNTs tend to aggregate in water with much precipitate on the bottom of the container, while the GONR/CNTs can be well dispersed in water and do not tangle together any more.

Due to the oxygen-containing functionalities such as carbonyls, carboxyls and hydroxyls exist at the edge and the surface of GONR/CNTs, the degree of the oxidation of GONR/CNTs was characterized by attenuated-total-reflection infrared (ATR-IR) spectroscopy, thermogravimetric analysis (TGA) and X-ray photoelectron spectroscopy (XPS). Compared with pristine MWCNTs, the ATR-IR spectroscopy (Figure S2) of GONR/CNTs clearly reveal the appearance of the C=O stretch ($\sim 1700 \text{ cm}^{-1}$) and the COO-H/O-H stretch ($\sim 3600\text{-}2800 \text{ cm}^{-1}$), and the XPS C1s spectrum in Figure 2 also presents the peaks of C-C, C-O and COOH in the GONR/CNTs structure. In addition, TGA shows the 7.9% and 48.3% weight loss of pristine MWCNTs and GONR/CNTs, respectively (Figure S3). The almost 50% weightlessness implies the presence of the carboxyl and hydroxyl functionalities in GONR/CNTs. The degree of the oxidation of GONR/CNTs is also clearly evaluated by the corresponding XPS C1s and O1s spectrum (Figure 2, Figure S4),³⁹ and a significant amount of oxygen is calculated to be 55.5 at%.

The successful partly unzipping of MWCNTs to GONR/CNTs can be further confirmed by XRD analysis and Raman spectra (Figure 3). As shown in Figure 3a, after oxidized by KMnO_4 and H_2SO_4 , GONR/CNTs show a peak at $\sim 10.8^\circ$ corresponding to the graphite (002) spacing, which does not exist in MWCNTs. This peak is mainly assigned to the formation of hydroxyl and carboxyl at the edge of GONR/CNTs, similar to that in graphene oxide. More importantly, XRD of GONR/CNTs appears a diffusion peak at $\sim 25.8^\circ$ where MWCNTs show a sharp peak. This indicates that the GONR/CNTs unzipped from MWCNTs are regular and stacked. In addition, MWCNTs before and after unzipping exhibit two characteristic peaks at 1353 and 1593 cm^{-1} in Raman spectra (Figure 3b), associated to the D and G peaks of CNTs, respectively. Compared with MWCNTs, GONR/CNTs show a stronger D peak, due to the oxidation of the MWCNTs. The conversion of MWCNTs to GONR/CNTs were also obviously evidenced by the variation of 2D band at $\sim 2700 \text{ cm}^{-1}$ from a sharp peak of carbon nanotubes to diffusion multi-peaks of multi-nanoribbons⁴⁰.

3.2 The electrochemical and optical bandgap of GONR/CNTs

Since GONR/CNTs can be regarded as a quasi-one-dimensional polymer,³⁵ the HOMO/LUMO energy levels of GONR/CNTs were conducted by cyclic voltammetry (CV). It was performed in a three electrode cell using platinum electrodes at a scan rate of 50 mV s^{-1} and an Ag/Ag^+ reference electrode in an anhydrous and nitrogen-saturated solution of 0.1 M tetrabutylammonium tetrafluoroborate (Bu_4NBF_4) in acetonitrile. Under these conditions, the onset oxidation potential ($E_{1/2\text{ox}}$) of ferrocene was -0.02 V versus Ag/Ag^+ . The HOMO energy level of the polymers was determined from the oxidation onset of the second scan from CV data. It is assumed that the redox potential of Fc/Fc^+ has an absolute energy level of -4.40 eV to vacuum. The energies of the HOMO and LUMO levels were calculated according to the following equations:

$$E_{\text{HOMO}} = -(\Phi_{\text{ox}} + 4.4) \text{ (eV)}$$

$$E_{\text{LUMO}} = -(\Phi_{\text{red}} + 4.4) \text{ (eV)}$$

where Φ_{ox} and Φ_{red} are the onset oxidation potential and the onset reduction potential

versus Ag/Ag^+ , respectively.^{41, 42} Introducing oxygen-rich groups around the GONR/CNT impact a significant effect on the bandgap of the resultant GONR/CNTs. As shown in Figure 4a, from the value of Φ_{ox} and Φ_{red} , the HOMO and LUMO energy levels GONR/CNTs are about -5.0 eV and -3.5 eV, respectively. The optical bandgap of GONR/CNTs was further measured by UV/Vis absorption spectrum. As shown in Figure S5, the absorb peak of GONR/CNTs appears at 235 nm and an onset of the spectrum appears at around 800 nm with a 1.5 eV bandgap. The results are similar with the literature reported,³⁵ which is also in consistent with the electrochemical bandgap.

3.3 The electrical properties of GONR/CNTs

To compare the conductivity of GONR/CNTs with pure GONR, the conductivity measurement was conducted with the structure of ITO/GONR/CNTs/Au and ITO/GONR/Au. The fabrication process is described in the experiment section. Their J - V characteristics are shown in Figure S6. As shown, the J - V curve exhibits a linear relationship with the voltage applied. The conductivities of the films were estimated from the slopes of the curve. It is obvious that GONR/CNTs exhibit a better conductivity than the pure GONR.

To measure the electrical properties of GONR/CNTs, the work function of the film was performed by Kelvin probe method, and the surface work function is displayed in Figure 4b. From the results we can find out that the GONR/CNTs-coated-ITO film shows a relatively high work function of 4.9 eV (see Figure 4b), which is equal to the HOMO levels of most polymer donors, such as P3HT (Figure 5a), thus it is suitable for hole transporting³⁵. To further exploit the application of GONR/CNTs in cathode modification, PEIE is attempted to be spin coated on the GONR/CNTs to lower its work function. Delightfully, after modified by a thin layer of PEIE (ca.10 nm), the work function of GONR/CNTs is dramatically reduced to 4.2 eV (Figure 4b) due to the neutral amine contained in PEIE creating interfacial dipole moment at the interface.^{36, 43} It makes a vacuum level shift about 0.7 eV, leading to a substantial change in the work function of GONR/CNTs, as shown in Figure 5b. The reduced

work function well matches, even better than ZnO (a work function of 4.5 eV), with the LUMO levels of the fullerene acceptor, to make the GONR/CNTs acting as ETL in PSCs. From energy level diagram of the device (Figure 5a) we can discover that the GONR/CNT employed as both HTL and ETL can construct a good energy level alignment in the device for charge extract, transport and collection.

3.4 Photovoltaic performance and characterization

By employing GONR/CNTs as interfacial layer, the solar cell devices with the structure of ITO/GONR/CNTs/PEIE/P3HT:PC₆₁BM/GONR/CNTs/Ag were fabricated to determine the function of GONR/CNTs (Figure 6). The molecular structures of P3HT, PC₆₁BM and PEIE, the device structure of modified GONR/CNTs and GONR/CNTs as interfacial layer are shown in Figure 6a and 6b. The GONR/CNTs layer was deposited by spin coating from its aqueous solution with a concentration of 3 mg mL⁻¹ to give a thickness of about 2 nm. The *J-V* characteristics of inverted polymer cells under AM 1.5G irradiation at 100 mW·cm⁻² are displayed in Figure 7, and the electrical parameters are listed in Table 1. The performance data is average 50 devices prepared on different days. The devices with ZnO as ETL and MoO₃ as HTL were also prepared as control device for comparison. As shown in Figure 7 and Table 1, the controlled device shows a PCE of ~3.1% with reasonable J_{sc} of 8.75 mA cm⁻², V_{oc} of 0.60 V and FF of 58%, in good agreement with the literature⁴⁴. When MoO₃ HTL is replaced by a thin layer of GONR/CNTs, the device delivers a comparable efficiency of ~3.0% to the control one, suggesting the effective anode modification of GONR/CNTs. More intriguingly, incorporation of GONR/CNTs/PEIE as ETL to replace ZnO, the device with configuration of ITO/GONR/CNTs/PEIE/P3HT:PC₆₁BM/MoO₃/Ag yield an all improved PCE of 3.7%, together with a J_{sc} of 9.16 mA cm⁻², a V_{oc} of 0.63 V and a FF of 0.64 V. The distinct improvement in PCE and corresponding parameters mainly results from the better energy alignment and the structure of GONR/CNTs with certain conductivity, as supported by energy level diagram in Figure 5.

Moreover, the organic/organic interface between GONR/CNTs/PEIE and

P3HT:PC₆₁BM favors an intimate contact and much more smooth morphology of P3HT:PC₆₁BM, which can be revealed by Figure 8. In view of the effective function of the GONR/CNT, the multifunctional nanoribbons are incorporated into the inverted devices as both HTL and ETL. As expected, the device with GONR/CNTs HTL and GONR/CNTs/PEIE ETL achieves remarkable improved PCE of 3.42%, with a J_{sc} of 8.53 mA cm⁻², V_{oc} of 0.63 V, and FF of 63%. Figure 7 shows the IPCE corresponding to the J - V characteristics. The device with GONR/CNTs based ETL and HTL shows the calculated J_{sc} of 8.28 mA cm⁻², which is well consistent with the J - V characteristics. To investigate the universality of the interfacial layer, PTB7:PC₇₁BM-based active layer was used to fabricate the device structure of ITO/ZnO/PTB7:PC₇₁BM/MoO₃/Ag and ITO/GONR/CNTs/PEIE/PTB7:PC₇₁BM/GONR/CNTs/Ag. As shown in Figure 9, the GONR/CNTs interfacial layer also worked well in PTB7:PC₇₁BM-based active layer invert solar cell. Compared with the ZnO and MoO₃ interfacial layer, the devices with GONR/CNTs as HTL and ETL achieved a remarkably improved PCE of 7.39%, with a J_{sc} of 14.65 mA cm⁻², V_{oc} of 0.73 V, and FF of 69%.

3.5 Evaluation of device stability.

Stability is an important factor for commercial application, hence the degradation of the device without any encapsulation in air (relative humidity ca. 15%; temperature ca. 22 °C) was observed for 30 days. Figure 10 shows the normalized efficiency of the inverted devices with the structure of ITO/GONR/CNTs/PEIE/P3HT:PC₆₁BM/GONR/CNTs/Ag and the structure of ITO/ZnO/P3HT:PC₆₁BM/MoO₃/Ag. Compared with ZnO and MoO₃, the GONR/CNTs interfacial layers ensure the devices with improved long-term stability. The PCE of the GONR/CNTs interfacial based layer device can be maintained 85% of its initial efficiency after storage time of 30 days, while the ZnO interfacial layer based device only strains 72% of its initial efficiency. We infer that the main reason for the stabilities of these devices is probably due to the morphology of the active layer. The morphology of P3HT:PCBM layer on GONR/CNTs/PEIE exhibits a better

surface with lower roughness than that on ZnO. Therefore, GONR/CNTs should be a potential interface material in high efficient and stable PSCs.

4. Conclusions

In conclusion, a low-cost and solution processible GONR/CNTs partially unzipped from MWCNTs was demonstrated. Unzipping of MWCNT can endow GONR/CNTs with continuous nanoribbons. What's more, GONR/CNTs have an open bandgap and its work function can easily be tuned by simple modification. As a result, with GONR/CNTs and PEIE modified GONR/CNTs as HTL and ETL, solution processed P3HT:PC₆₁BM-based and PTB7:PC₇₁BM-based PSCs achieves a high PCE of 3.42% and 7.39%, respectively. These results are even higher than the ZnO ETL and MoO₃ HTL based device. Furthermore, GONR/CNTs interlayer also ensures the device with a significant high stability. Therefore, the multifunctional GONR/CNTs unzipped from MWCNTs would be a promising interfacial materials for solution processed high performance PSCs. Moreover, after further reducing, such GONR/CNTs are also expected to have the potential for electrode application due to the high conductivity.

Supporting Information

The detailed experimental sections and the corresponding characterization are in Supporting Information. This information is available free of charge via the Internet at <http://pubs.rsc.org>.

Acknowledgements

This work was financially supported by the National Science Fund for Distinguished Young Scholars (51425304), National Natural Science Foundation of China (51273088, 51263016 and 51473075), and National Basic Research Program of China (973 Program 2014CB260409).

References

1. N. S. Sariciftci, L. Smilowitz, A. J. Heeger and F. Wudl, *Science*, 1992, **258**, 1474-1476.
2. G. Li, V. Shrotriya, J. S. Huang, Y. Yao, T. Moriarty, K. Emery and Y. Yang, *Nat. Mater.*, 2005, **4**, 864-868.
3. G. Yu, J. Gao, J. C. Hummelen, F. Wudl and A. J. Heeger, *Science*, 1995, **270**, 1789-1791.
4. T. B. Yang, W. Z. Cai, D. H. Qin, E. G. Wang, L. F. Lan, X. Gong, J. B. Peng and Y. Cao, *J. Phys. Chem. C*, 2010, **114**, 6849-6853.
5. P. W. M. Blom, V. D. Mihailetschi, L. J. A. Koster and D. E. Markov, *Adv. Mater.*, 2007, **19**, 1551-1566.
6. http://www.nrel.gov/ncpv/images/efficiency_chart.jpg (2015.02.09 data)
7. K. D. G. I. Jayawardena, L. J. Rozanski, C. A. Mills, M. J. Beliatas, N. A. Nismy and S. R. P. Silva, *Nanoscale*, 2013, **5**, 8411-8427.
8. Y. Y. Liang, Z. Xu, J. B. Xia, S. T. Tsai, Y. Wu, G. Li, C. Ray and L. P. Yu, *Adv. Mater.*, 2010, **22**, E135-E138.
9. J. B. You, L. T. Dou, K. Yoshimura, T. Kato, K. Ohya, T. Moriarty, K. Emery, C. C. Chen, J. Gao, G. Li and Y. Yang, *Nat. Commun.*, 2013, **4**, 1446
10. H. L. Yip, S. K. Hau, N. S. Baek, H. Ma and A. K. Y. Jen, *Adv. Mater.*, 2008, **20**, 2376-2382.
11. J. Y. Kim, S. H. Kim, H. H. Lee, K. Lee, W. L. Ma, X. Gong and A. J. Heeger, *Adv. Mater.*, 2006, **18**, 572-576.
12. A. C. Arango, L. R. Johnson, V. N. Bliznyuk, Z. Schlesinger, S. A. Carter and H. H. Horhold, *Adv. Mater.*, 2000, **12**, 1689-1692.
13. M. S. White, D. C. Olson, S. E. Shaheen, N. Kopidakis and D. S. Ginley, *Appl. Phys. Lett.*, 2006, **89**, 143517.
14. J. B. You, C. C. Chen, L. T. Dou, S. Murase, H. S. Duan, S. A. Hawks, T. Xu, H. J. Son, L. P. Yu, G. Li and Y. Yang, *Adv. Mater.*, 2012, **24**, 5267-5272.
15. H. Choi, J. S. Park, E. Jeong, G. H. Kim, B. R. Lee, S. O. Kim, M. H. Song, H. Y. Woo and J. Y. Kim, *Adv. Mater.*, 2011, **23**, 2759-2763.
16. Y. X. Zhu, X. F. Xu, L. J. Zhang, J. W. Chen and Y. Cao, *Sol. Energy Mater. Sol. Cells*, 2012, **97**, 83-88.
17. T. B. Yang, M. Wang, C. H. Duan, X. W. Hu, L. Huang, J. B. Peng, F. Huang and X. Gong, *Energy Environ. Sci.*, 2012, **5**, 8208-8214.
18. Q. L. Bao and K. P. Loh, *Acs Nano*, 2012, **6**, 3677-3694.
19. D. S. Yu, Y. Yang, M. Durstock, J. B. Baek and L. M. Dai, *Acs Nano*, 2010, **4**, 5633-5640.
20. K. P. Loh, Q. L. Bao, P. K. Ang and J. X. Yang, *Journal of Materials Chemistry*, 2010, **20**, 2277-2289.
21. C. X. Guo, G. H. Guai and C. M. Li, *Adv. Energy Mater.*, 2011, **1**, 448-452.
22. P. H. Wobkenberg, G. Eda, D. S. Leem, J. C. de Mello, D. D. C. Bradley, M. Chhowalla and T. D. Anthopoulos, *Adv. Mater.*, 2011, **23**, 1558-1562.
23. E. Kymakis, K. Savva, M. M. Stylianakis, C. Fotakis and E. Stratakis, *Adv. Funct. Mater.*, 2013, **23**, 2742-2749.

24. G. Kakavelakis, D. Konios, E. Stratakis and E. Kymakis, *Chem. Mater.*, 2014, **26**, 5988-5993.
25. L. Zhang, J. J. Liang, Y. Huang, Y. F. Ma, Y. Wang and Y. S. Chen, *Carbon*, 2009, **47**, 3365-3368.
26. F. Bonaccorso and Z. P. Sun, *Opt. Mater. Express*, 2014, **4**, 63-78.
27. Y. Gao, H.-L. Yip, S. K. Hau, K. M. O'Malley, N. C. Cho, H. Chen and A. K.-Y. Jen, *Appl. Phys. Lett.*, 2010, **97**, 203306.
28. J. Liu, Y. Xue, Y. Gao, D. Yu, M. Durstock and L. Dai, *Adv. Mater.*, 2012, **24**, 2228-2233.
29. D. V. Kosynkin, A. L. Higginbotham, A. Sinitskii, J. R. Lomeda, A. Dimiev, B. K. Price and J. M. Tour, *Nature*, 2009, **458**, 872-875.
30. A. L. Higginbotham, D. V. Kosynkin, A. Sinitskii, Z. Z. Sun and J. M. Tour, *Acs Nano*, 2010, **4**, 2059-2069.
31. Y. W. Son, M. L. Cohen and S. G. Louie, *Phys. Rev. Lett.*, 2006, **97**, 216803.
32. M. Y. Han, B. Ozyilmaz, Y. B. Zhang and P. Kim, *Phys. Rev. Lett.*, 2007, **98**, 206805.
33. X. L. Li, X. R. Wang, L. Zhang, S. W. Lee and H. J. Dai, *Science*, 2008, **319**, 1229-1232.
34. L. M. Xie, H. L. Wang, C. H. Jin, X. R. Wang, L. Y. Jiao, K. Suenaga and H. J. Dai, *J. Am. Chem. Soc.*, 2011, **133**, 10394-10397.
35. J. Liu, G. H. Kim, Y. H. Xue, J. Y. Kim, J. B. Baek, M. Durstock and L. M. Dai, *Adv. Mater.*, 2014, **26**, 786-790.
36. Y. H. Zhou, C. Fuentes-Hernandez, J. Shim, J. Meyer, A. J. Giordano, H. Li, P. Winget, T. Papadopoulos, H. Cheun, J. Kim, M. Fenoll, A. Dindar, W. Haske, E. Najafabadi, T. M. Khan, H. Sojoudi, S. Barlow, S. Graham, J. L. Bredas, S. R. Marder, A. Kahn and B. Kippelen, *Science*, 2012, **336**, 327-332.
37. Y. M. Sun, J. H. Seo, C. J. Takacs, J. Seifter and A. J. Heeger, *Adv. Mater.*, 2011, **23**, 1679-1683.
38. D. Li, M. B. Muller, S. Gilje, R. B. Kaner and G. G. Wallace, *Nat. Nanotech.*, 2008, **3**, 101-105.
39. Y. W. Zhu, S. Murali, W. W. Cai, X. S. Li, J. W. Suk, J. R. Potts and R. S. Ruoff, *Adv. Mater.*, 2010, **22**, 5226-5226.
40. A. C. Ferrari, J. C. Meyer, V. Scardaci, C. Casiraghi, M. Lazzeri, F. Mauri, S. Piscanec, D. Jiang, K. S. Novoselov, S. Roth and A. K. Geim, *Phys. Rev. Lett.*, 2006, **97**, 187401.
41. C. P. Chen, S. H. Chan, T. C. Chao, C. Ting and B. T. Ko, *J. Am. Chem. Soc.*, 2008, **130**, 12828-12833.
42. Q. D. Zheng, B. J. Jung, J. Sun and H. E. Katz, *J. Am. Chem. Soc.*, 2010, **132**, 5394-5404.
43. A. K. K. Kyaw, D. H. Wang, V. Gupta, J. Zhang, S. Chand, G. C. Bazan and A. J. Heeger, *Adv. Mater.*, 2013, **25**, 2397-2402.
44. M. T. Dang, L. Hirsch and G. Wantz, *Adv. Mater.*, 2011, **23**, 3597-3602.

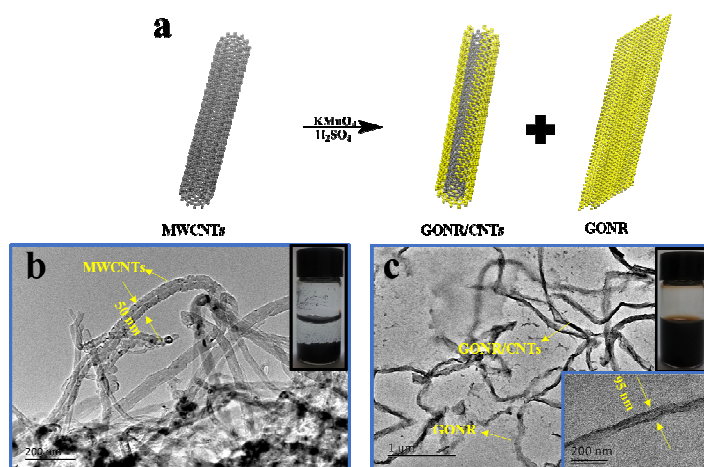


Fig. 1 (a) The simplified synthesis process of the GONR/CNTs. (b) TEM image of pristine MWCNTs and (c) GONR/CNTs. Insert digital images shows the pristine MWCNTs and GONR/CNTs dispersed in water, respectively.

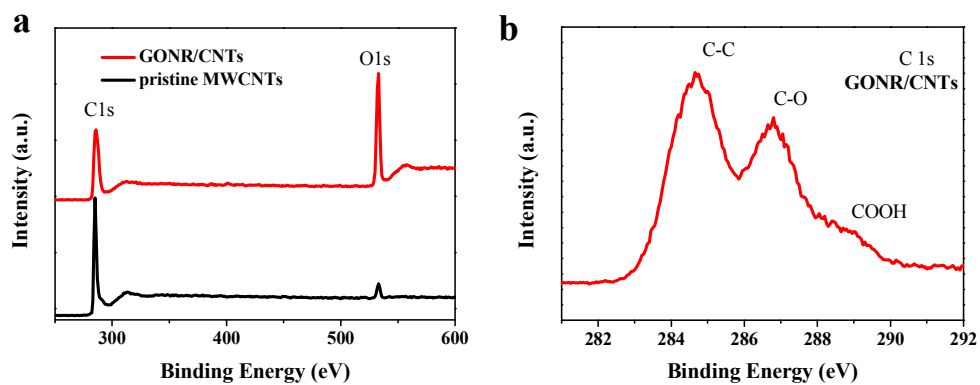


Fig. 2 XPS characterization of carbon based materials. (a) XPS survey spectra of GONR/CNTs and pristine MWCNTs, (b) XPS carbon 1s spectra of GONR/CNTs.

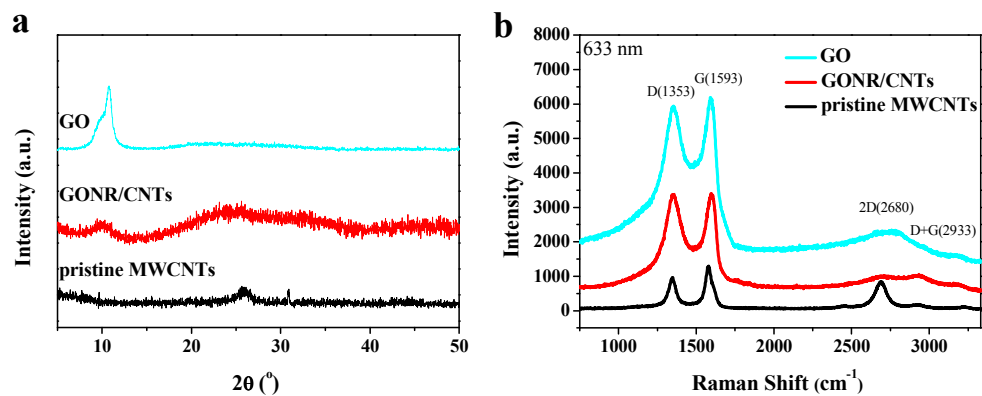


Fig. 3 (a) X-ray diffraction of GO, GONR/CNTs and pristine MWCNTs. θ , diffraction angle; a.u., arbitrary units. (b) The Raman spectra of GO, GONR/CNTs and pristine MWCNTs at 633 nm.

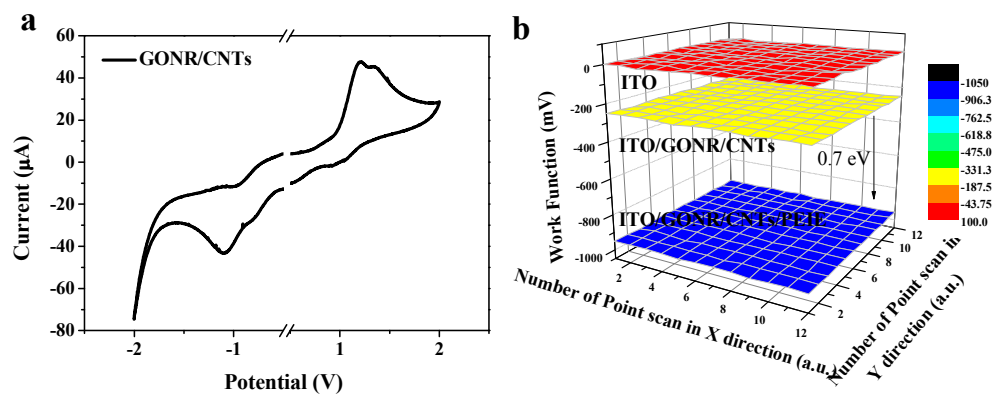


Fig. 4 (a) Cyclic voltammetry of GONR/CNTs drop-cast on a Pt electrode in 0.1 mol L⁻¹ Bu₄NPF₆-acetonitrile solutions at a scan rate of 50 mV/s. (b) Work function of bare ITO, GONR/CNTs-coated-ITO and PEIE-coated-GONR/CNTs measured by Kelvin probe method.

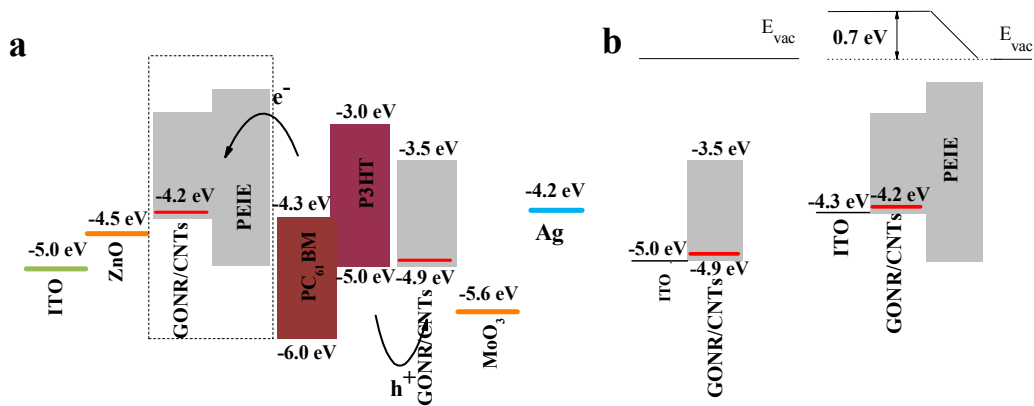


Fig. 5 (a) Energy level diagram of the materials used in inverted devices. (b) Illustration of vacuum level shift and reduced work function of GONR/CNTs-coated-ITO after deposition of PEIE layer.

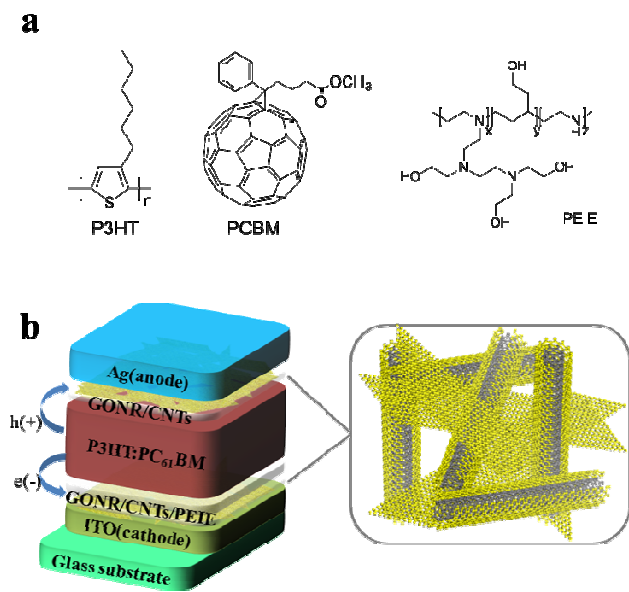


Fig. 6 (a) Structure of P3HT and PC₆₁BM. (b) Schematic illustration of the P3HT:PC₆₁BM BHJ-based PSC device with GONR/CNTs as the HTL and ETL, and the insert shows the structure of GONR/CNTs in the film.

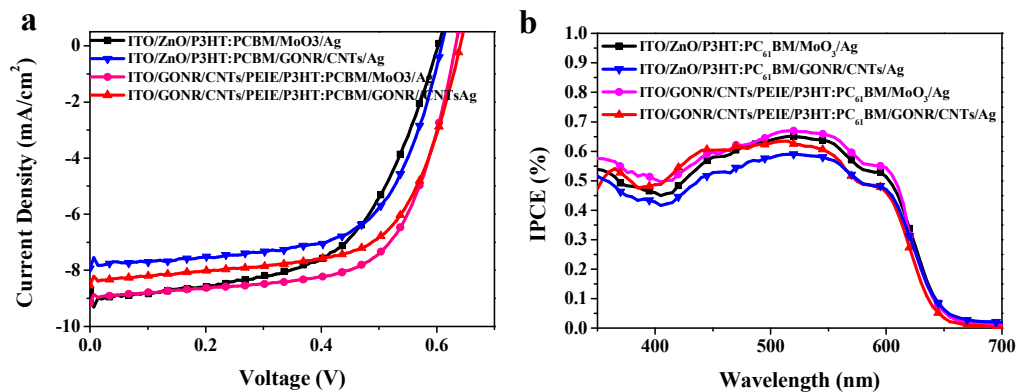


Fig. 7 (a) J - V characteristics of P3HT:PC₆₁BM-based active layer inverted cells with various cathode interfacial layers under AM 1.5G irradiation at 100 mW/cm². (b) Incident photo-to-electron conversion efficiency (IPCE) spectra of the inverted devices with the various ETLs and HTLs.

Table 1 Summary of the photovoltaic performance of inverted P3HT:PC₆₁BM solar cells with various ETLs and HTLs.

Device Structure ^a	J_{sc} [mA/cm ²]	V_{oc} [V]	FF	PCE [%]
ITO/ZnO/P3HT:PC ₆₁ BM/MoO ₃ /Ag	8.75 ±0.25	0.60 ±0.01	0.58±0.01	3.10 ±0.07
ITO/ZnO/P3HT:PC ₆₁ BM/GONR/CNTs/Ag	7.93 ±0.22	0.61 ±0.01	0.62 ±0.01	3.00 ±0.09
ITO/GONR/CNTs/PEIE/P3HT:PC ₆₁ BM/MoO ₃ /Ag	9.16 ±0.22	0.63 ±0.01	0.64 ±0.01	3.70 ±0.09
ITO/GONR/CNTs/PEIE/P3HT:PC ₆₁ BM/GONR/CNTs /Ag	8.53 ±0.24	0.63 ±0.01	0.63 ±0.01	3.42 ±0.08

^a All the devices of this work: all values represent averages from six 4 mm² devices on 50 devices prepared on different days on single chip measuring under AM 1.5 with 100 mW/cm² irradiation.

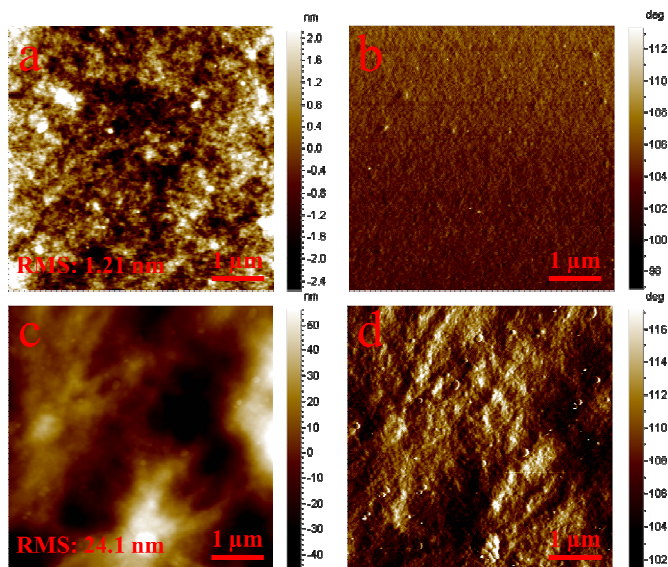


Fig. 8 AFM height and phase images of P3HT:PC₆₁BM film on (a,b) ITO/GONR/CNTs/PEIE ETL and (c,d) ITO/ZnO ETL. And (a,c) are the height images, (b,d) are the phase images. The scan size is 5 μm × 5 μm and scan rate is 1 Hz for all images.

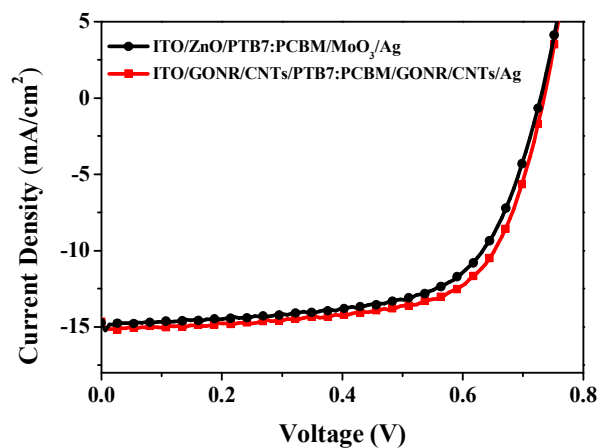


Fig. 9 (a) J - V characteristics of PTB7:PC₇₁BM-based active layer inverted cells with various cathode interfacial layers under AM 1.5G irradiation at 100 mW/cm².

Table 2 Summary of the photovoltaic performance of inverted PTB7:PC₇₁BM-based solar cells with various ETLs and HTLs.

Device Structure ^a	J_{sc} [mA/cm ²]	V_{oc} [V]	FF	PCE [%] ^b
ITO/ZnO/PTB7:PC ₇₁ BM/MoO ₃ /Ag	14.73±0.57	0.73±0.01	0.65±0.02	6.97±0.11
ITO/GONR/CNTs/PEIE/PTB7:PC ₇₁ BM/GONR/CNTs /Ag	14.65±0.45	0.73±0.01	0.69±0.03	7.39±0.13

^adevice configuration: glass/ITO/ETL/PTB7:PC₇₁BM (1:1.5 w/w, 130-180 nm)/HTL/Ag (90 nm). ^bAll the PCE were averaged over 15 devices.

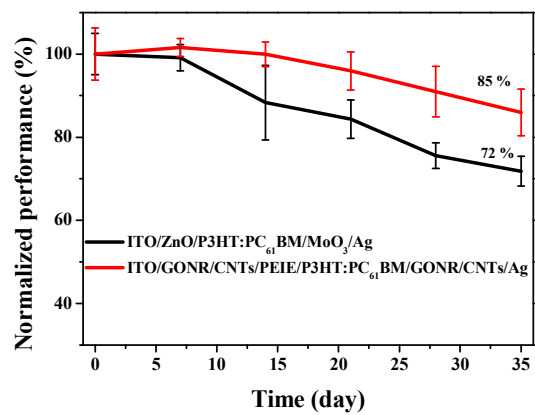


Fig. 10 Normalized PCE of inverted devices with the structure of ITO/GONR/CNTs/PEIE/P3HT:PC₆₁BM/GONR/CNTs/Ag and ITO/ZnO/P3HT:PC₆₁BM/MoO₃/Ag as a function of storage time in air without any encapsulation.

Table of contents for**One-dimension Graphene Nanoribbons Hybridized with Carbon Nanotubes as Cathode and Anode Interfacial Layers for High Performance Solar Cells**

Yong Zhang, Yawen Liu, Lie Chen, Xiaotian Hu, Lin Zhang, Lin Hu, Yiwang Chen*

Introducing the GONR/CNTs into the solution processed PSCs as ETL and HTL simultaneously delivers a high performance with long-term stability.

Graphical abstract